

Article

Growing and Etching MoS₂ on Carbon Nanotube Film for Enhanced Electrochemical Performance

Weiyu Xu [†], Qi Fang [†], Daobin Liu, Ke Zhang, Muhammad Habib, Chuanqiang Wu, Xusheng Zheng, Hengjie Liu, Shuangming Chen and Li Song ^{*}

National Synchrotron Radiation Laboratory, CAS Center for Excellence in Nanoscience, University of Science and Technology of China, Hefei 230029, China; xuweiyu@mail.ustc.edu.cn (W.X.); fq4311@mail.ustc.edu.cn (Q.F.); ldbin@mail.ustc.edu.cn (D.L.); zk2009@mail.ustc.edu.cn (K.Z.); mhabib@mail.ustc.edu.cn (M.H.); wucq@mail.ustc.edu.cn (C.W.); zxs@ustc.edu.cn (X.Z.); lhjbh@mail.ustc.edu.cn (H.L.); csm@ustc.edu.cn (S.C.)

^{*} Correspondence: song2012@ustc.edu.cn; Tel.: +86-551-6360-2102

[†] These authors contributed equally to this paper.

Academic Editor: Saikat Talapatra

Received: 5 September 2016; Accepted: 28 September 2016; Published: 30 September 2016

Abstract: In this work we directly synthesized molybdenum disulfide (MoS₂) nanosheets on carbon nanotube film (MoS₂@CNT) via a two-step chemical vapor deposition method (CVD). By etching the obtained MoS₂@CNT into 10% wt HNO₃, the morphology of MoS₂ decorated on CNT bundles was modulated, resulting in more catalytic active MoS₂ edges being exposed for significantly enhanced electrochemical performance. Our results revealed that an 8 h acid etching sample exhibited the best performance for the oxygen evolution reaction, i.e., the current density reached 10 mA/cm² under 375 mV over-potential, and the tafel slope was as low as 94 mV/dec. The enhanced behavior was mainly originated from the more catalytic sites in MoS₂ induced by the acid etching treatment and the higher conductivity from the supporting CNT films. Our study provides a new route to produce two-dimensional layers on CNT films with tunable morphology, and thus may open a window for exploring its promising applications in the fields of catalytic-, electronic-, and electrochemical-related fields.

Keywords: carbon nanotube; molybdenum disulfide; CVD; acid etching; electrochemical performance

1. Introduction

Growing industrialization and the immense use of energy which is usually obtained from fossil fuels create a significant harmful impact on the climate and human health. Due to rapid exhaustion of fossil energy and environmental concerns, people are now exerting enormous efforts to develop renewable energy sources such as solar energy [1–4], wind power [5–7] and bioenergy [8–12], etc. Hydrogen generated by splitting water has a great potential as an ideal future energy source because of its high energy density and lack of toxicity features. The water splitting process can be divided into two half-processes [13], the hydrogen evolution reaction (HER) and the oxygen evolution reaction (OER). Because of the energy and dynamic barrier, to drive the reaction on, a potential higher than 1.23 V is essential. Between these two half-processes, OER is the bottleneck because of the multi-proton transfer process [14]. Introduction of a catalyst can significantly reduce this over-potential, thus resulting in improved energy conversion efficiency. Iridium oxidate is the best catalyst for OER [13] but its practical uses suffers from high price and low earth abundance, while transition metal compounds can overcome these two disadvantages and can be a good substitution to catalyze the OER reaction according to the volcano plot [13].

Molybdenum disulfide (MoS₂), a typical layered transition metal dichalcogenide (TMDC), which has a 1.29 eV indirect bandgap in the bulk state and a 1.8 eV direct bandgap in the monolayer state [15],

is not only the ideal candidate for future semiconductor materials [15–17], but also a suitable catalyst in the electrochemical catalytic field [18,19] and a lithium battery anode material [20–22]. There are three shortcomings which hinder the practical use of MoS₂ as a catalyst in the water splitting process. First, as a typical semiconductor, MoS₂ has quite poor conductivity, which causes poor electron transfer ability. Second, because of the tension strength released during the catalyzing process, catalysts are not stable. To solve these two problems, composites containing MoS₂ with a substrate such as reduced graphene oxide [23], carbon nanotubes [20], or nickel foam [24], etc., have been developed and tested. Such substrates provide an excellent electron conducting network and stabilize the MoS₂ in the network. Third, bulk MoS₂ has few active sites. Reducing the size of the MoS₂ is a feasible method to increase the active sites. There are a lot of research works focusing on the synthesis of MoS₂ nano-flowers [25], nano-sheets [26] and nano-rods [27] or introducing defects such as unsaturated sulfur [28] to enhance the catalyzing performance. Most of those works are based on the hydrothermal method.

In our previous work, we synthesized a non-woven carbon nanotube film (CNT film) with a good mechanical property and high conductivity [28]. Herein, we employed such a CNT film as a supporting material, and used a developed chemical vapor deposition method to directly grow MoS₂ on the CNT film for preparing hybridized structures (MoS₂@CNT). As follows, an acid treatment with 10% wt HNO₃ was also supposed to reduce the thickness and tune the morphology of the obtained MoS₂ nanosheets in order to create more active catalytic sites in the MoS₂ being exposed. Meanwhile, the entangled nanotube bundles among the CNT film can further accelerate the transport of electrons. Therefore, such deliberate processes will open up a new way for producing high-performance synergistic hybrid materials for enhanced electrochemical performance.

2. Results

2.1. Synthesis and Characterization of MoS₂@CNT Composite

Our CVD configuration that has been used to synthesize CNT film and MoS₂@CNT [29] is shown in Figure 1a,b. The detailed synthesis process can be found in our previous work [30] and is also described in the following Materials and Methods section.

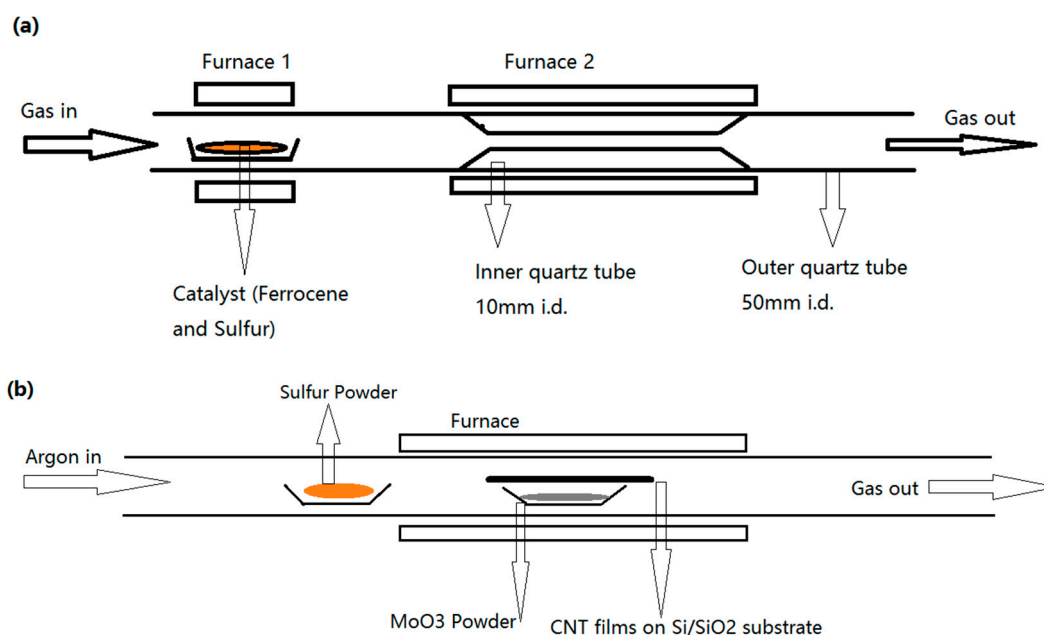


Figure 1. Schematic route of the CVD configuration used to grow: (a) CNT film; and (b) MoS₂@CNT hybrids.

Scanning electronic microscopy (SEM) characterization results are shown in Figure 2a–d. In the as-grown MoS₂@CNT sample, MoS₂ with a pillar-like structure stacks layer by layer, thus forming thick coverage on top of the CNT film. The thick MoS₂ layer has poor conductivity and fewer active sites for catalysis, which decreased the electrochemical performance. To reduce the thickness of the MoS₂ cover, as-grown MoS₂@CNT samples were treated with 10% wt. HNO₃ for different durations. By controlling the treatment duration, we suggest that the thickness and morphology of MoS₂ can be selectively modulated; hence, the electrochemical catalysis performance will be subsequently optimized. The experimental results for different durations of acid etching are shown in Figure 2b–d. After 2 h treatment the MoS₂ layer thickness has been significantly reduced, thus exposing the network structure of the CNT film which is illustrated in Figure 2b. By extending the acid etching duration to 8 h (Figure 2c), the pillar structure can be further dissolved and the MoS₂ coverage area is considerably diminished. When we increased the acid etching duration to 12 h, most of the MoS₂ coverage was removed from the CNT film surface and the clear nanotube network structure remained, as shown in Figure 2d. In fact, there is still MoS₂ retention detected from the Raman spectroscopy in Figure 3a and the X-ray photoelectron spectrum (XPS) in Figure 4a,c.

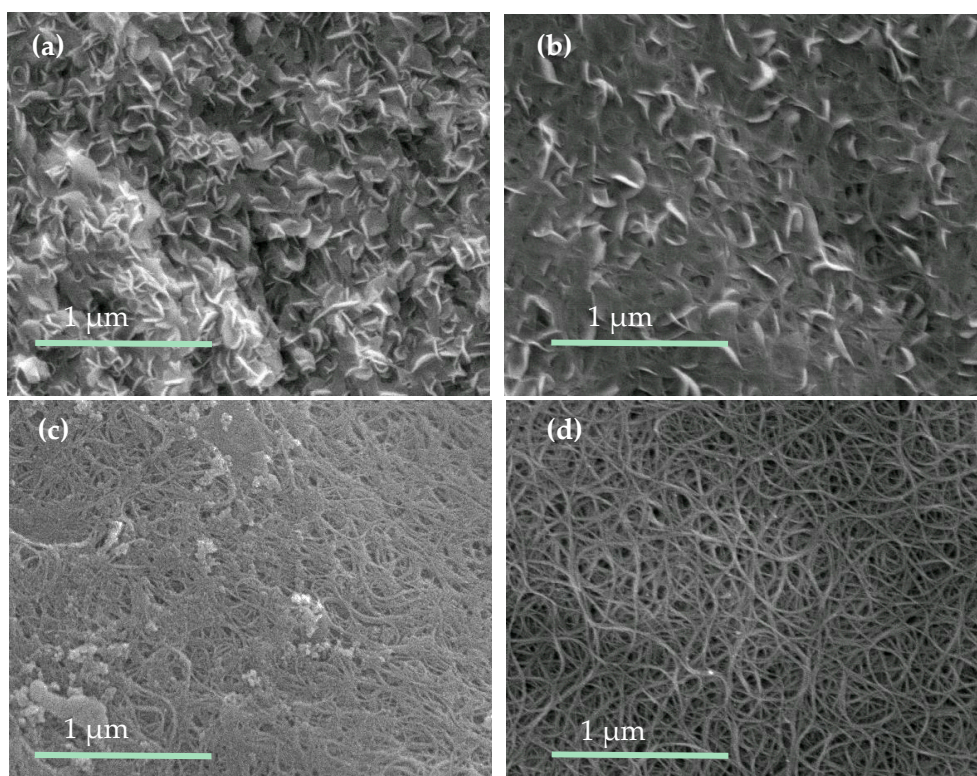


Figure 2. SEM surface morphology of MoS₂@CNT composite: (a) pristine sample and (b–d) treated with 10% wt. HNO₃ for 2 h, 8 h, and 12 h.

The Raman spectrum is a very useful tool to identify the existence of MoS₂ [31]. Figure 3a shows the typical Raman spectra of pristine MoS₂@CNT and acid-treated MoS₂@CNT with different treatment durations. From the Raman spectra it can be observed that there are two main peak regions; one is at around 100–300 cm⁻¹ which corresponds to the radial breathing mode (RBM) of single-wall carbon nanotubes [30], while the other is at 300–450 cm⁻¹ and is related to the MoS₂. The zoom-in and deconvolution results in Figure 3b clearly show two distinguishable vibration modes of MoS₂, the in-plane vibration mode E_{2g}¹ (~383 cm⁻¹ for bulk MoS₂) and the out-of-plane vibration mode A_{1g} (~405 cm⁻¹ for bulk MoS₂). The intensity of the E_{2g}¹ and A_{1g} peaks was decreased with the increase of the HNO₃ etching duration. Although the intensity of those two vibration modes was significantly

decreased for samples treated for 12 h, their detection in the spectra reveals the existence of MoS₂ at the CNT surface which is also confirmed by the following XPS results.

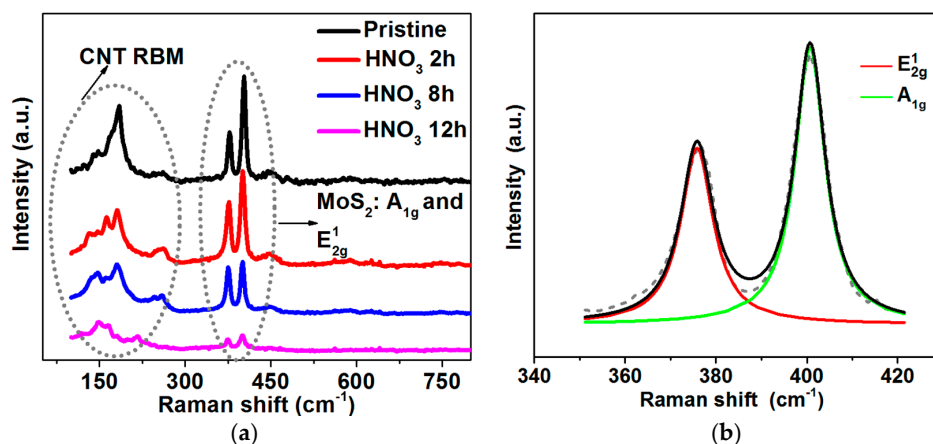


Figure 3. Raman spectrum of MoS₂@CNT: (a) Pristine and treated samples with HNO₃ for 2 h, 8 h and 12 h. (b) Deconvolution results of pristine MoS₂@CNT for E_{2g}¹ and A_{1g} modes.

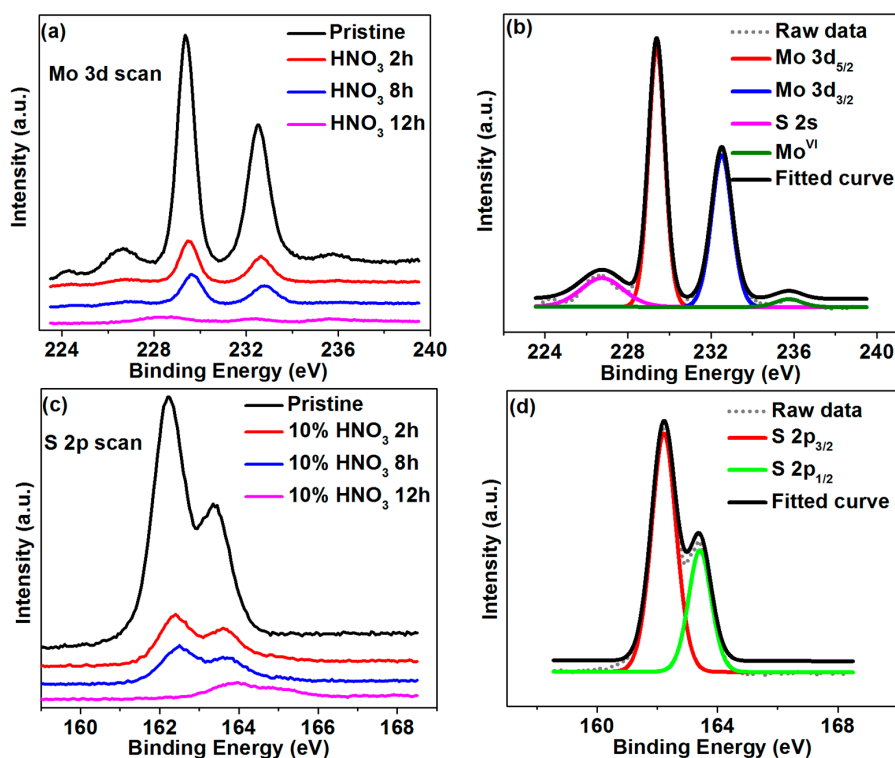


Figure 4. XPS results of different samples: (a,c) Mo 3d and S 2p curve comparison among different durations of acid-treated (pristine, 2 h, 8 h, 12 h) MoS₂@CNT, and (b,d) pristine MoS₂@CNT Mo 3d and S 2p deconvolution.

Figure 4 shows the XPS characterization of different-acid-etching-duration samples. The calibration was done by referencing all XPS spectra to the C (1s) peak in Figure S3. In the as-grown MoS₂@CNT samples, typical Mo 3d_{5/2} (at 229.4 eV), Mo 3d_{3/2} (at 232.5 eV), together with highly oxidized Mo (MoO₃ at 235.8 eV), can be seen in the deconvoluted curves [24,28]. It is worth noting that the atomic ratio of Mo and S in the as-grown MoS₂@CNT is 1:2.14, calculated from Figure 4b,d.

With the increase of the HNO₃ etching duration, Mo 3d and S 2p bonding became smaller and broadened, which means that the atomic ratios of these atoms were decreased. Meanwhile, the highly oxidized Mo peak disappeared, referring to the fact that MoO₃ was reacted and dissolved in the HNO₃ solution. Those phenomena showed that MoS₂ has been etched away during acid treatment, which was also proved by the above SEM characterization (Figure 2b–d).

The surface Molybdenum (Mo) and carbon (C) atomic ratio calculated from Figure 4a and Figure S3 with an integrated peak surface area and sensitive factor correlation [32] can refer to the relative MoS₂ component on the CNT film substrate surface, as shown in Table 1. With the increase of the HNO₃ etching duration, MoS₂ on the CNT film surface reduces significantly.

Table 1. Surface Mo and C atomic ratio of different HNO₃ etching duration samples.

Atomic Ratio	Pristine	10% wt HNO ₃ 2 h	10% wt HNO ₃ 8 h	10% wt HNO ₃ 12 h
Surface Mo and C atomic ratio	1.555	0.073	0.047	0.009

2.2. Electrochemical Performance Test of MoS₂@CNT Composite

The electrochemical measurements of MoS₂@CNT have been carried out with 1 M NaOH as an electrolyte and Hg/HgO as a reference electrode. Our results are shown in Figure 5. All data has been converted to a reversible hydrogen electrode (RHE). As shown in Figure 5a, the linear sweep voltammetry (LSV) results have been corrected by IR compensate.

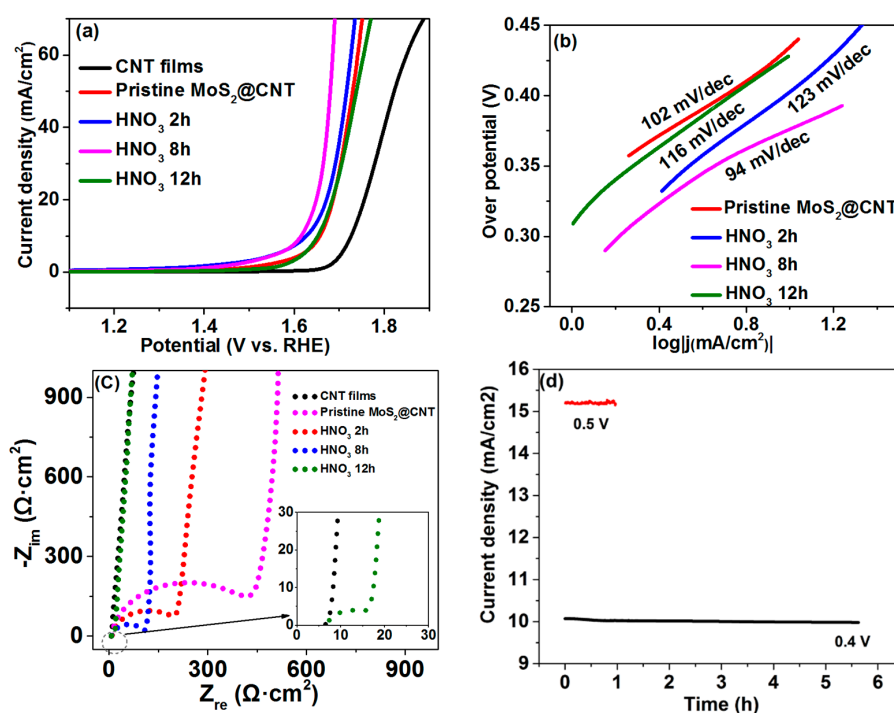


Figure 5. Electrochemical performances of different acid etching MoS₂@CNT: (a) LSV curves of CNT film, pristine MoS₂@CNT, MoS₂@CNT treated with HNO₃ for 2 h, 8 h and 12 h; and (b) corresponding tafel slope; (c) Impedance curves of pristine MoS₂@CNT, MoS₂@CNT treated with HNO₃ for 2 h, 8 h and 12 h; (d) Current-time plot of the 8 h HNO₃ etching duration MoS₂@CNT.

Obviously, the MoS₂@CNT exhibited a better OER catalyzing performance as compared to the CNT film. With the increase of the HNO₃ etching duration, the MoS₂@CNT catalyzing performance showed significant improvement, but after a certain point, the performance was decreased.

The required over-potential when the current density reaches 10 mA/cm² is 504 mV, 435 mV, 404 mV, 375 mV and 428 mV for CNT film, pristine MoS₂@CNT, and MoS₂@CNT treated with HNO₃ for 2 h, 8 h and 12 h.

From Figure 5b, with the increase of the acid etching duration, the tafel slope of MoS₂@CNT showed clear changes. In particular, the 8 h acid-treated sample had the smallest tafel slope, suggesting the best dynamic process among those etching samples. Impedance tests were performed on the samples, as shown in Figure 5c. Pristine MoS₂@CNT showed a 400 Ω electron transfer resistance (R_{ct}). With the increase of the acid etching duration, R_{ct} decreased gradually, as expected. The inserted curve of Figure 5c revealed that the CNT film has a very small R_{ct} (~5 Ω), which can promote the catalyzing performance. Based on the above data, Figure 5d showed the catalytic performance stability of the HNO₃ etching duration MoS₂@CNT samples. The catalytic performance showed a slight decrease after a 6 h test under a 0.4 V over-potential. When increasing this over-potential to 0.5 V, the current density can reach 15 mA/cm. However, after a 1 h test, the current density dropped rapidly, which means the catalytic stability decreased.

3. Discussion

The pristine MoS₂@CNT has a fairly thick MoS₂ layer, thus it has fewer active sites (Figure 2a) and poor electron transfer ability (Figure 5c). When treated with 10% wt. HNO₃, the MoS₂ reacted with HNO₃ and formed MoO₃, and then MoO₃ further reacted with HNO₃ and was dissolved into the solution. The possible mechanism can be elucidated with the following chemical process [33].



After etching with acid for different time durations, the MoS₂ layer was etched gradually; also the layer integrity was destroyed, as shown in the SEM results (Figure 2b,c), which was further proved by the transmission electron microscopy (TEM) results (Figure 6a). More MoS₂ edges were exposed which resulted in more active sites (Figure 6b). Meanwhile, the reduction of the layer thickness can guarantee sufficient contact between the MoS₂ and CNT film; hence, the electron conductivity could be greatly improved. In fact, a further increased acid etching duration (more than 8 h) can further enhance the electron transfer ability, but the active sites decreased significantly, resulting in a poor catalyzing performance (Figures 2d and 5a).

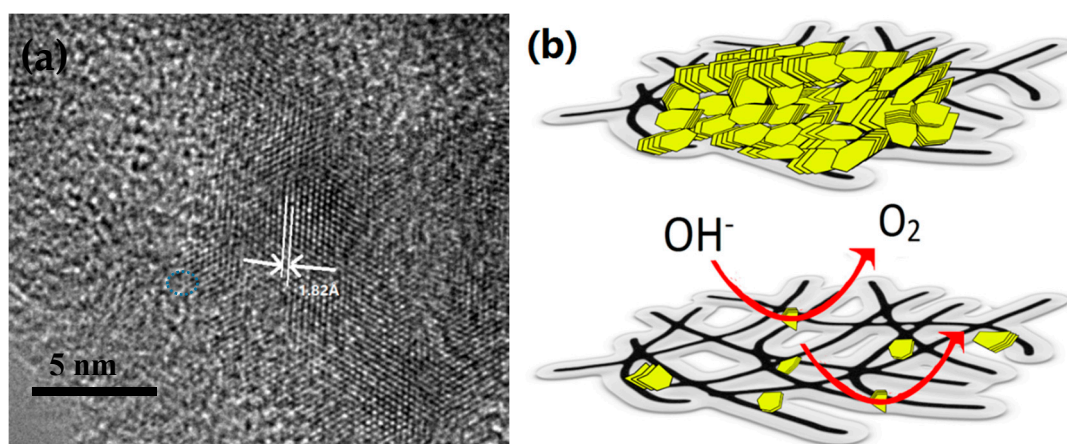


Figure 6. TEM images of MoS₂@CNT: (a) high magnification image of MoS₂@CNT and 1.82 Å is referred to the 2H-MoS₂ (105) plane [34]. (b) Schematic illustration of: top, pristine MoS₂@CNT and bottom, etching MoS₂@CNT OER process. Black network refers to CNT film and yellow sheets refer to MoS₂.

4. Materials and Methods

MoO₃ (99.5%) was purchased from Alfa Aesar (Yingong RD No. 229, Fengxian Chemical District, Shanghai, China), The other reagents were purchased from Sinopharm Chemical Reagent Co. Ltd. (Ningbo RD No. 22, Shanghai, China): Sulfur (99.999%), Ferrocene (98%), Ethanol (AR), HCl (37%, AR), and HNO₃ (66%, AR). All chemical reagents have been purchased from company and used without further purification.

4.1. Synthesis of CNT Film

Carbon nanotube film was synthesized by a floating CVD method as reported before [30]. The configuration is shown in Figure 1a. A special designed 50 mm diameter quartz tube with a 10 mm diameter inner tube was placed in furnace (MTK Co. Ltd., Hefei, China) and extra heating belt was set to heat the catalyst (16:1 molar ratio Ferrocene:S).

CNT film has been prepared by the following temperature process: main heating zone was heated to 1000 °C with a 30 °C/min ramping rate and a 200 sccm argon airflow was introduced as protective atmosphere. Next, temperature was increased to 1100 °C with 10 °C/min rate and at the same time second furnace was set to heat the catalyst at 90 °C. On reaching to 1100 °C, argon flow was increased to 1000 sccm and mixed with 3 sccm methane flow. After two hours of growth time, furnace was stopped and cooled to room temperature naturally. The as prepared CNT film has a high stretchable big size as shown in Figure S1.

The as-grown CNT film was first oxidized at 300~400 °C for 12~24 h to remove amorphous carbon, then immersed in 37% HCl for seven days to get rid of iron particles induced by ferrocene. After these purification steps, a clean random carbon nanotube network could be seen as shown in Figure S2. The purified CNT film was stored in ethanol.

4.2. Synthesis of MoS₂@CNT

To get a uniform MoS₂ layer on CNT film, first extended CNT film in Distilled Water and then transfer on Si/SiO₂ substrate. After drying in oven at 90 °C, CNT film was placed upside down on a ceramic boat where deposited 14 mg MoO₃. As shown in Figure 1b, ceramic boat was place in the middle of furnace, and at the edge of furnace hot zone, another boat with 120 mg sulfur powder was placed.

The growing process can be described as following steps. First 1000 sccm argon flow was introduced to get rid of air remaining in quartz tube. After 10 min argon rinsing, increased temperature to 750 °C with a 50 °C/min ramping rate, and MoS₂ growth time lasted for 2 min at this temperature. After growing process was finished, to ensure good MoS₂ structure, furnace has been opened to cool the quartz tube rapidly.

As-grown MoS₂@CNT was treated in 10% wt. HNO₃ for different times to etch MoS₂ layer. After treated with HNO₃, MoS₂@CNT can be peeled off from Si/SiO₂ substrate for next characterizations and testing steps.

4.3. Characterizations

Scanning Electron Microscopy (SEM). A field emission scanning electron microscope (SEM 15 kV, JEOL, JSM-6700F, Tokyo, Japan).

X-ray Photoelectron Spectroscopy (XPS, AXIS-HIS, Kratos Analytical, Hadano, Japan). The Photoemission Endstation at the BL10B beamline in the National Synchrotron Radiation Laboratory (NSRL) in Hefei, China.

Transmission electron microscopy (TEM). A field emission transmission electron microscope (TEM 200 kV, JEOL, JEM-2100F, Tokyo, Japan).

X-ray Diffraction (XRD, Japanese Rigaku Company, Tokyo, Japan). A D8-Advance power diffractometer with a Cu-K α radiation source ($\lambda = 1.54178 \text{ \AA}$).

Raman Spectra. A Horiba microscopic Raman spectrometer (XploRA, HORIBA, Ltd., Tokyo, Japan). The laser having wavelength 532 nm (~ 2.5 mW/cm²) over a range of 70–3000 cm⁻¹.

4.4. Electrochemical Measurements

All the electrochemical measurements were carried out with an electrochemical workstation (CHI660D electrochemical workstation) in a standard three-electrode cell with Hg/HgO and Pt mesh as the reference electrode and counter electrode, respectively. A glassy carbon (GC) electrode (3 mm in diameter) acted as the working electrode. OER measurements were conducted in 1 M NaOH as the electrolyte, which was saturated with oxygen during the experiments. The LSVs were performed at a scanning rate of 5 mV/s. The EIS spectrum was carried out with a 5 mV perturbative potential. The amperometric *i-t* curve was carried out with the same test condition as LSV scan.

5. Conclusions

In summary, we have employed a purified non-woven CNT film as a supporting material for directly growing MoS₂ on it with the CVD method. The obtained samples showed hybridized structures with thick MoS₂ nanosheets decorated on the CNT bundles. By etching the obtained MoS₂@CNT with 10% wt. HNO₃, the morphology of MoS₂ has been tuned to expose more catalytic active sites. Meanwhile, the contact between the MoS₂ and CNT film became tighter; hence, the electron transfer ability has been improved. The synergistic effect subsequently enhanced the electrochemical performance for OER catalysis. This work shows a possibility to directly prepare CNT-based hybrids and provides a way to tune the electron structure of the hybrids with acid treatment. Considering the fact that CVD method can be easily conducted for industrial producing, this study with the CVD growth and acid-etching process may be quite essential for future CNT-based electrochemical and electronic applications.

Supplementary Materials: Supplementary materials can be accessed at: <http://www.mdpi.com/1420-3049/21/10/1318/s1>.

Acknowledgments: We acknowledge the financial support from the National Basic Research Program of China (2014CB848900), NSF (U1232131, U1532112, 11375198, 11574280), CUSF (WK2310000053), User with Potential from CAS Hefei Science Center (2015HSC-UP020). L.S. thanks the recruitment program of global experts, the CAS Hundred Talent Program. We also thank the Hefei Synchrotron Radiation Facility (MCD, photoemission and Catalysis/Surface Science Endstations, NSRL), and the USTC Center for Micro and Nanoscale Research and Fabrication for help in characterizations and fabrications.

Author Contributions: Weiyu Xu and Qi Fang conceived and designed the experiments; Qi Fang performed the experiments; Weiyu Xu analyzed the data and wrote the paper; Daobin Liu and Ke Zhang contributed analysis tools and guidance; Chuanqiang Wu contributed TEM characterization; Muhammad Habib contributed materials; Xusheng Zheng and Shuangming Chen contributed XPS experiment and analysis. Henjie Liu contributed electrochemical test help; Song Li is the designer and supervisor of the project. All authors discussed and wrote the manuscript.

Conflicts of Interest: The authors declare no conflict of interest.

References

1. Green, M.A.; Emery, K.; Hishikawa, Y.; Warta, W.; Dunlop, E.D. Solar cell efficiency tables (Version 45). *Prog. Photovolt. Res. Appl.* **2015**, *23*. [[CrossRef](#)]
2. Lenert, A.; Wang, E.N. Optimization of nanofluid volumetric receivers for solar thermal energy conversion. *Sol. Energy* **2012**, *86*, 253–265.
3. Mei, A.; Li, X.; Liu, L.; Ku, Z.; Liu, T.; Rong, Y.G.; Xu, M.; Chen, J.Z.; Yang, Y. A hole-conductor-free, fully printable mesoscopic perovskite solar cell with high stability. *Science* **2014**, *345*, 295–298. [[CrossRef](#)] [[PubMed](#)]
4. You, J.; Dou, L.; Yoshimura, K.; Kato, T.; Ohya, K.; Moriarty, T.; Emery, K.; Chen, C.C.; Gao, J.; Li, G.; et al. A polymer tandem solar cell with 10.6% power conversion efficiency. *Nat. Commun.* **2013**, *4*. [[CrossRef](#)] [[PubMed](#)]

5. Díaz-González, F.; Sumper, A.; Gomis-Bellmunt, O.; Villafafila-Robles, R. A review of energy storage technologies for wind power applications. *Renew. Sustain. Energy Rev.* **2012**, *16*, 2154–2171. [[CrossRef](#)]
6. Hirth, L. The market value of variable renewables. *Energy Econ.* **2013**, *38*, 218–236. [[CrossRef](#)]
7. Zhao, H.; Wu, Q.; Hu, S.; Xu, H.; Rasmussen, C.N. Review of energy storage system for wind power integration support. *Appl. Energy* **2015**, *137*, 545–553. [[CrossRef](#)]
8. Follett, R.F.; Vogel, K.P.; Varvel, G.E.; Mitchell, R.B.; Kimble, J. Soil Carbon Sequestration by Switchgrass and No-Till Maize Grown for Bioenergy. *BioEnergy Res.* **2012**, *5*, 866–875. [[CrossRef](#)]
9. Gelfand, I.; Saphajpal, R.; Zhang, X.; Izaurralde, R.C.; Fross, K.L.; Robertson, G.P. Sustainable bioenergy production from marginal lands in the US Midwest. *Nature* **2013**, *493*, 514–517. [[CrossRef](#)] [[PubMed](#)]
10. Jones, C.S.; Mayfield, S.P. Algae biofuels: Versatility for the future of bioenergy. *Curr. Opin. Biotechnol.* **2012**, *23*, 346–351. [[CrossRef](#)] [[PubMed](#)]
11. Meier, D.; Beld, D.V.B.; Bridgwater, A.V.; Elliott, D.C.; Oasmaa, A.; Preto, F. State-of-the-art of fast pyrolysis in IEA bioenergy member countries. *Renew. Sustain. Energy Rev.* **2013**, *20*, 619–641. [[CrossRef](#)]
12. Mullet, J.; Morishige, D.; McCormick, R.; Truong, S.; Hilley, H.; McKinley, B.; Anderson, R.; Olson, S.; Rooney, W. Energy sorghum—A genetic model for the design of C4 grass bioenergy crops. *J. Exp. Bot.* **2014**, *65*, 3479–3489. [[CrossRef](#)] [[PubMed](#)]
13. Greeley, J.; Markovic, N.M. The road from animal electricity to green energy: Combining experiment and theory in electrocatalysis. *Energy Environ. Sci.* **2012**, *5*. [[CrossRef](#)]
14. Diaz-Morales, O.; Ledezma-Yanez, I.; Koper, M.T.M.; Calle-Vallejo, F. Guidelines for the Rational Design of Ni-Based Double Hydroxide Electrocatalysts for the Oxygen Evolution Reaction. *ACS Catalysis* **2015**, *5*, 5380–5387. [[CrossRef](#)]
15. Buscema, M.; Barkelid, M.; Zwiller, V.; Zant, H.S.; Steele, G.A.; Castellanos-Gomez, A. Large and tunable photothermoelectric effect in single-layer MoS₂. *Nano Lett.* **2013**, *13*, 358–363. [[CrossRef](#)] [[PubMed](#)]
16. Castellanos-Gomez, A.; Cappelluti, E.; Roldán, R.; Agrait, N.; Guinea, F.; Rubio-Bollinger, G. Electric-field screening in atomically thin layers of MoS₂: The role of interlayer coupling. *Adv. Mater.* **2013**, *25*, 899–903. [[CrossRef](#)] [[PubMed](#)]
17. Chuang, S.; Battaglia, C.; Azcatl, A.; McDonnell, S.; Kang, J.S.; Yin, X.; Tosun, M.; Kapadia, R.; Fang, H.; Mallace, R.M.; et al. MoS₂ P-type transistors and diodes enabled by high work function MoO_x contacts. *Nano Lett.* **2014**, *14*, 1337–1342. [[CrossRef](#)] [[PubMed](#)]
18. Chen, Z.; Cummins, D.; Reinecke, B.N.; Clark, E.; Sunkara, M.K.; Jaramillo, T.F. Core-shell MoO₃-MoS₂ nanowires for hydrogen evolution: A functional design for electrocatalytic materials. *Nano Lett.* **2011**, *11*, 4168–4175. [[CrossRef](#)] [[PubMed](#)]
19. Drescher, T.; Niefind, F.; Bensch, W.; Grunert, W. Sulfide catalysis without coordinatively unsaturated sites: Hydrogenation, cis-trans isomerization, and H₂/D₂ scrambling over MoS₂ and WS₂. *J. Am. Chem. Soc.* **2012**, *134*, 18896–18899. [[CrossRef](#)] [[PubMed](#)]
20. Bindumadhavan, K.; Srivastava, S.K.; Mahanty, S. MoS₂-MWCNT hybrids as a superior anode in lithium-ion batteries. *Chem. Commun.* **2013**, *49*, 1823–1825. [[CrossRef](#)] [[PubMed](#)]
21. Chang, K.; Chen, W. In situ synthesis of MoS₂/graphene nanosheet composites with extraordinarily high electrochemical performance for lithium ion batteries. *Chem Commun.* **2011**, *47*, 4252–4254. [[CrossRef](#)] [[PubMed](#)]
22. Chang, K.; Geng, D.; Li, X.; Yang, J.; Tang, Y.; Cai, M.; Li, R.; Sun, X. Ultrathin MoS₂/Nitrogen-Doped Graphene Nanosheets with Highly Reversible Lithium Storage. *Adv. Energy Mater.* **2013**, *3*, 839–844. [[CrossRef](#)]
23. Li, Y.; Wang, H.; Xie, L.; Liang, Y.; Hong, G.; Dai, H. MoS₂ nanoparticles grown on graphene: An advanced catalyst for the hydrogen evolution reaction. *J. Am. Chem. Soc.* **2011**, *133*, 7296–7299. [[CrossRef](#)] [[PubMed](#)]
24. Yan, K.; Lu, Y. Direct Growth of MoS₂ Microspheres on Ni Foam as a Hybrid Nanocomposite Efficient for Oxygen Evolution Reaction. *Small* **2016**, *12*, 2975–2981. [[CrossRef](#)] [[PubMed](#)]
25. Hu, S.; Chen, W.; Zhou, J.; Yin, F.; Uchaker, E.; Zhang, Q.; Cao, G. Preparation of carbon coated MoS₂ flower-like nanostructure with self-assembled nanosheets as high-performance lithium-ion battery anodes. *J. Mater. Chem. A* **2014**, *2*. [[CrossRef](#)]
26. Voiry, D.; Salehi, M.; Silva, R.; Fujita, T.; Chen, M.; Asefa, T.; Shenoy, V.B.; Eda, G.; Chhowalla, M. Conducting MoS₂ nanosheets as catalysts for hydrogen evolution reaction. *Nano Lett.* **2013**, *13*, 6222–6227. [[CrossRef](#)] [[PubMed](#)]

27. Tian, Y.; Zhao, J.; Fu, W.; Liu, Y.; Zhu, Y.; Wang, Z. A facile route to synthesis of MoS₂ nanorods. *Mater. Lett.* **2005**, *59*, 3452–3455. [[CrossRef](#)]
28. Liu, D.; Xu, W.; Liu, Q.; He, Q.; Haleem, Y.A.; Xiang, T.; Zou, C.; Chu, W.; Zhong, J.; Niu, Z.; et al. Unsaturated-sulfur-rich MoS₂ nanosheets decorated on free-standing SWNT film: Synthesis, characterization and electrocatalytic application. *Nano Res.* **2016**, *9*, 2079–2087. [[CrossRef](#)]
29. Shi, Y.; Li, H.; Li, L.J. Recent advances in controlled synthesis of two-dimensional transition metal dichalcogenides via vapour deposition techniques. *Chem. Soc. Rev.* **2015**, *44*, 2744–2756. [[CrossRef](#)] [[PubMed](#)]
30. Song, L.; Ci, L.; Lv, L.; Zhou, Z.; Yan, X.; Liu, D.; Yuan, H.; Gao, Y.; Wang, J.; Liu, L. Direct synthesis of a macroscale single-walled carbon nanotube non-woven material. *Adv. Mater.* **2004**, *16*. [[CrossRef](#)]
31. Li, H.; Zhang, Q.; Yap, C.C.; Tay, B.K.; Edwin, T.H.; Olivier, A.; Baillargeat, D. From Bulk to Monolayer MoS₂: Evolution of Raman Scattering. *Adv. Funct. Mater.* **2012**, *22*, 1385–1390. [[CrossRef](#)]
32. Burrow, B.J. A correlation of Auger electron spectroscopy, X-ray photoelectron spectroscopy, and Rutherford backscattering spectrometry measurements on sputter-deposited titanium nitride thin films. *J. Vac. Sci. Technol. A* **1986**, *4*. [[CrossRef](#)]
33. Amara, K.K.; Chu, L.; Kumar, R.; Toh, M.; Eda, G. Wet chemical thinning of molybdenum disulfide down to its monolayer. *APL Mater.* **2014**, *2*. [[CrossRef](#)]
34. Shariza, S.; Anand, T.J.S. Effect of Deposition Time on the Structural and Optical Properties of Molybdenum Chalcogenides Thin Films. *Chalcogenide Lett.* **2011**, *8*, 529–539.

Sample Availability: Samples of the compounds are available from the authors.



© 2016 by the authors; licensee MDPI, Basel, Switzerland. This article is an open access article distributed under the terms and conditions of the Creative Commons Attribution (CC-BY) license (<http://creativecommons.org/licenses/by/4.0/>).